

## AlMg6–AlMg6 weld interface: microstructure and mechanical properties after explosive welding

© Andrey Yu. Malakhov<sup>a</sup>, Ivan V. Saikov<sup>a</sup>, Igor V. Denisov<sup>a</sup>,  
**Alexander A. Berdychenko<sup>b</sup>**, Sergey G. Ivanov<sup>b</sup>, Nemat N. Niyozbekov<sup>a</sup>✉

<sup>a</sup> Merzhanov Institute of Structural Macrokinetics and Materials Science RAS (ISMAN),  
8, Academician Osipyan St., Chernogolovka, 142432, Russian Federation,  
<sup>b</sup> Polzunov Altai State Technical University, 46, Lenin Ave., Barnaul, 656038, Russian Federation

✉ nemat199595@mail.ru

**Abstract:** Due to their low density, high strength, and resistance to corrosion, Al-Mg alloys are widely used in the railcar construction and shipbuilding, and other industries. The aim of this study was to carry out a detailed analysis of the microstructure of the AlMg6–AlMg6 weld interface after explosive welding (EW). The results of this study are important for a better understanding of the joint formation process in EW of AlMg6 with other metals and alloys. The study included optical and electron microscopy of metallographic specimens with etched surfaces. Vickers hardness tests and tear strength tests were carried out to determine the mechanical properties of the joint. Optical and electron microscopy revealed a large number of adiabatic shear bands (ASBs) formed during EW and dark-etching structures formed after etching. An increase in explosive welding parameters leads to an increase in ASBs in the flyer plate and parent plate. The dark-etching structures are most likely the accumulations of structural defects and intermetallic compound fragments. The tear testing of the weld joint showed that higher EW parameters lead to much higher tear strength with a non-uniform distribution along the length of the plates. It was concluded that in order to achieve a joint between AlMg6 and other alloys and metals with the highest strength, plastic deformation in the weld interface must be sufficiently high, while heating must be minimal. The maximum joint strength was 150 MPa in mode 2 and 242 MPa in mode 3, respectively.

**Keywords:** Al–Mg alloys; explosive welding; weld interface; microstructure.

**For citation:** Malakhov AYu, Saikov IV, Denisov IV, **Berdychenko AA**, Ivanov SG, Niyozbekov NN. AlMg6–AlMg6 weld interface: microstructure and mechanical properties after explosive welding. *Journal of Advanced Materials and Technologies*. 2023;8(4):304-315. DOI: 10.17277/jamt.2023.04.pp.304-315

## Граница соединения АМг6–АМг6: микроструктура и механические свойства после сварки взрывом

© А. Ю. Малахов<sup>a</sup>, И. В. Сайков<sup>a</sup>, И. В. Денисов<sup>a</sup>,  
**А. А. Бердыченко<sup>b</sup>**, С. Г. Иванов<sup>b</sup>, Н. Н. Ниязбеков<sup>a</sup>✉

<sup>a</sup> Институт структурной макрокинетики и проблем материаловедения  
им. А. Г. Мерджанова РАН, ул. Академика Осипяна, 8, Черноголовка, 142432, Российская Федерация,  
<sup>b</sup> Алтайский государственный технический университет им. И.И. Ползунова,  
пр. Ленина, 46, Барнаул, 656038, Российская Федерация

✉ nemat199595@mail.ru

**Аннотация:** Сплавы системы Al–Mg широко используются в судостроении, вагоностроении и других отраслях промышленности благодаря низкой плотности, высокой прочности и коррозионной стойкости. Цель работы – проведение детального исследования микроструктуры границы соединения АМг6–АМГ6 после сварки взрывом. Результаты исследования позволили лучше понимать процесс формирования соединений при сварке взрывом сплава АМг6 с другими металлами и сплавами. Металлографические исследования образцов проводили

с помощью оптической и электронной микроскопии. Для исследования механических свойств проведены испытания прочности на отрыв и измерена микротвердость слоев. Оптическая и электронная микроскопия показала, что в процессе сварки взрывом в материалах образуются полосы адиабатического сдвига. Увеличение параметров сварки взрывом приводит к увеличению полос адиабатического сдвига в метаемом и основном слое. Также на границе соединения были обнаружены темнотравящиеся структуры. Предположительно такие структуры представляют собой скопления дефектов и интерметаллических соединений. Установлено, что для получения прочного соединения АМг6 с другими металлами и сплавами необходимо обеспечить пластическую деформацию свариваемых поверхностей при минимальном нагреве зоны соединения. Максимальная прочность соединения составила 150 МПа по режиму 2 и 242 МПа по режиму 3, соответственно.

**Ключевые слова:** сплав АМг6; сварка взрывом; граница соединения; микроструктура.

**Для цитирования:** Malakhov AYu, Saikov IV, Denisov IV, Berdychenko AA, Ivanov SG, Niyozbekov NN. AlMg6–AlMg6 weld interface: microstructure and mechanical properties after explosive welding. *Journal of Advanced Materials and Technologies*. 2023;8(4):304-315. DOI: 10.17277/jamt.2023.04.pp.304-315

## 1. Introduction

The metals and alloys that contribute to reducing the weight of constructions have been in high demand in the aerospace, shipbuilding, automotive and railcar industries. Aluminum alloys are the most commonly used materials for such applications due to their light weight, suitable mechanical properties and corrosion resistance, as well as good weld ability and workability. Wrought non-heat treatable aluminum alloys of the Al–Mg system are currently widely used because of their good corrosion resistance in many acids and seawater, as well as their high tensile strength (up to 420 MPa). These excellent performance properties are due to solid solution strengthening.

It is not always advisable to make constructions entirely of Al–Mg alloys due to their low stiffness and low melting points compared to steel or titanium. Therefore, the elements of a construction that undergo significant mechanical stresses are often made of steel or other alloys. For example, in the shipbuilding industry, the ship hull is made of steel, whereas chimney casings, wheelhouses and deck bridges are made of Al–Mg alloys. This reduces the overall ship weight up to 50–60 %, thus increasing the deadweight tonnage and improving the overall ship performance [1, 2]. In particular, the hovercraft hulls are made entirely of Al–Mg alloys. In the automotive industry, Al–Mg alloys are used in manufacturing various parts of suspension, transmissions, etc. [3]. This reduces the automobile's weight and fuel consumption and minimizes CO<sub>2</sub> emissions [4]. In addition, Al–Mg alloys are used in the production of cryogenic equipment used in the transportation of liquefied gases [5].

Nowadays, various fusion welding methods are used for joining Al–Mg alloys to steel work pieces [6].

Pressure welding produces stronger joints between Al–Mg alloys and steels compared to fusion

welding. This is due to the fact that the joint is formed in the solid phase, which significantly reduces the number of brittle Fe<sub>x</sub>Al<sub>y</sub> IMCs at the weld interface. The joint between Al–Mg alloy and steel can be made by friction welding [7, 8], diffusion welding [9], ultrasonic welding [10], cold rolling [11], magnetic-pulse welding [12], hot isostatic pressing [13], and explosive welding (EW) [14–16].

All those studies have shown that the welding of aluminum alloys with steels poses a number of challenges. These challenges are associated with brittle Fe<sub>x</sub>Al<sub>y</sub> IMCs, the differences in the melting points of the two metals, their physical properties and thermal expansion coefficients. Therefore, bimetallic transition joints (BTJ) are used to meet these challenges [17]. Consequently, the properties of the BTJs used in the process of welding will define a construction's overall performance properties.

Nowadays, EW is a promising technique for the BTJs manufacturing [17, 18]. For example, G. Costanza et al. welded a BTJ consisting of 5086 aluminum alloy and A516 steel with an intermediate layer of pure aluminum [19]. A new method of EW of 5083 aluminum alloy with Q345 steel was studied in [20], where dovetail grooves were employed. The tensile shear strength of 5083/Q345 clad plate was 167.6 MPa, that is higher than that of 5083 aluminum alloy. However, the dovetail grooves trapped the compressed gas in the gap between the base and flyer plates, which led to the formation of pores in the weld interface.

Microstructure and morphology of the weld interface are important characteristics in EW studies. The weld interface morphology is divided into wavy interface [21] and straight interface [22, 23]. The weld interface microstructure can vary significantly in depth due to the non-uniform heat distribution, namely, the heat does not have time to dissipate from locally heated zones, which are formed

**Table 1.** Mechanical properties and chemical composition of commercial AlMg6 alloy under EN 10204 3.2 certificate

Tensile strength, MPa		Yield strength, MPa		Elongation, %		Density, kg·m <sup>-3</sup>					
353-356		193-221		16.6–19.3		2640					
Composition, wt. %											
Al		Mg		Mn		Zn		Fe		others	
92.73		5.80–5.87		0.86		0.18		0.16		0.20	

due to highly intensive deformation of the weld interface. Also, this deformation causes very high grain refinement near the weld interface [24], thus the process of structure fragmentation takes place [25]. The structure fragmentation was studied in detail in [26]. In addition, numerous deformation twins, dislocations and adiabatic shear bands (ASBs) near the weld interface were observed in many studies [27–29]. EW of dissimilar metals produces brittle IMCs and solid solutions at the weld interface [30], which, in most cases, significantly reduce the strength of the welded joint [31].

The main objective in the BTJ production is to achieve the tensile strength comparable to that of AlMg6. Obtaining a strong joint between steel and pure aluminum does not pose many difficulties. On the other hand, the strong joint between steel and Al–Mg alloys cannot be achieved if the magnesium content is greater than 5 % [32, 33]. As is known, magnesium is the main factor that defines the mechanical properties of AlMg6 [34].

Resolving these issues requires detailed study of the structure of the weld interface in the AlMg6 bimetal. Such a scheme excludes the formation of Fe<sub>x</sub>Al<sub>y</sub> IMCs, thus allowing to determine the effects of magnesium on the weld interface formation. This scheme of joining similar metals was applied in [35] where the EW of Al to Al was performed.

This study examined the EW of AlMg6 with AlMg6. It presented the results of the microstructural study of the AlMg6–AlMg6 weld interface after EW and the results of the mechanical testing of the joint. These results will be used in further studies to determine the parameters of the EW of AlMg6 alloy with steels.

## 2. Materials and Methods

### 2.1. Initial materials

The initial materials used in this study were 4-mm-thick plates of AlMg6 alloy, whose composition and properties are listed in Table 1.

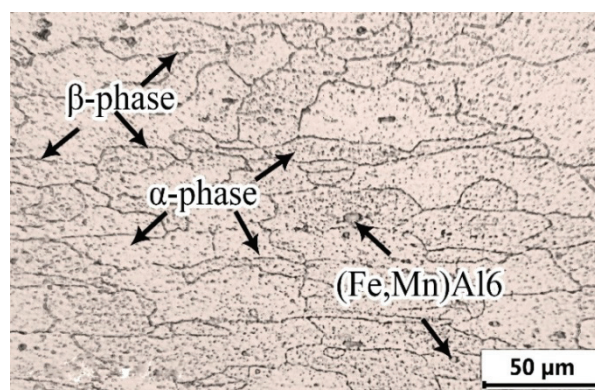
**Fig. 1.** The initial microstructure of the AlMg6

Figure 1 shows the microstructure of the initial AlMg6 plate. The grains of  $\alpha$ -solid solution ( $\alpha$ -phase) are elongated along the rolling direction. Small (Fe, Mn)Al<sub>6</sub> inclusions are inside the grains, whereas  $\beta$ -phase (Mg<sub>2</sub>Al<sub>3</sub>) is along the grain boundaries [36].

### 2.2. Explosive welding

The EW experiments were conducted in the parallel plate configuration shown in Fig. 2a. Before assembling, the surfaces of the plates were cleaned from oxide films and rust. The explosive used was a 96 : 4 mixture of microporous ammonium nitrate and diesel oil ( $d = 780 \text{ kg·m}^{-3}$ ). The top surface of the flyer plate was covered with a protective polythene layer. The layer of the explosive was spread over the configuration, placed in a formwork (Fig. 2b), and exploded with a detonator.

The EW parameters were calculated from the equations taken from [37]. The equation for the flyer plate velocity is given as follows:

$$V_0 = 1.2D \frac{\sqrt{1 + \frac{32}{27}r - 1}}{\sqrt{1 + \frac{32}{27}r + 1}}, \quad (1)$$

where  $D$  is the detonation velocity,  $\text{m·s}^{-1}$ ;  $r$  is the ratio of the explosive mass to the flyer plate mass:



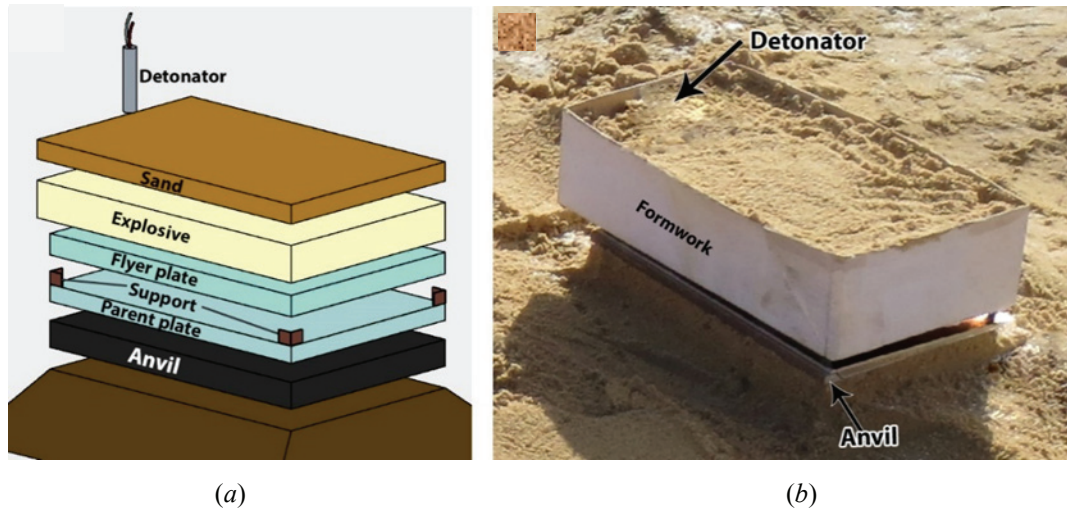


Fig. 2. Configuration of the experiment (a) and actual view of the experiment (b)

$$r = \frac{m_e}{m_{pl}}, \quad (2)$$

where  $m_e$  is the explosive mass, kg;  $m_{pl}$  is the flyer plate mass, kg.

The collision angle was calculated from the following equation:

$$\gamma = 2 \arcsin \left( \frac{V_0}{2D} \right). \quad (3)$$

### 2.3. Microstructural study

The tear strength specimens and metallographic specimens were prepared according to Fig. 3.

The specimens with approximate dimensions of  $30 \times 30 \times 8$  mm were cut from zone B, the specimens with approximate dimensions of  $10 \times 20 \times 8$  mm – from zones A.

The metallographic specimens were embedded into a BAKELIT GF conductive compound with graphite filler using a METAPRESS-P metallographic

press. Grinding and polishing were performed using a DIGIPREP machine. Grinding was carried out using emery papers of grit sizes 320, 800, 1500 and 2500. Polishing was carried out using two water-based suspensions. One suspension contained  $3 \mu\text{m}$  diamond particles, while the other contained  $1 \mu\text{m}$  diamond particles. Super finishing was carried out in an acid suspension of colloidal silicon oxide with a particle size of  $0.05 \mu\text{m}$ . The identification of microstructural elements was performed by successive etching with Keller's reagent for 5–15 s and then with Vek's reagent for 60 s [38–40].

The metallographic studies were performed with a Carl Zeiss Axio Observer Z1m inverted metallographic microscope using a Thixomet Pro software package according to the procedure given in [41–44]. The SEM/EDS analysis was carried out with a Zeiss Ultraplus microscope equipped with an INCA 350 Oxford accessory.

### 2.4. Mechanical testing

The microhardness (HV) was measured using a PMT-3 Vickers hardness tester and MMS software. Loads of 50 g were applied for 10 s. Figure 4 shows a microhardness measurement diagram.

The tear testing of the weld joint after EW was conducted on an Instron 1195 universal testing machine as shown in Fig. 5.

Then tear strength  $\sigma_t$  was calculated from the following equation:

$$\sigma_t = \frac{4P}{\rho(d_2^2 - d_1^2)}, \quad (4)$$

where  $P$  is the applied load, N;  $d_1$  is the inner diameter, mm;  $d_2$  is the outer diameter, mm.

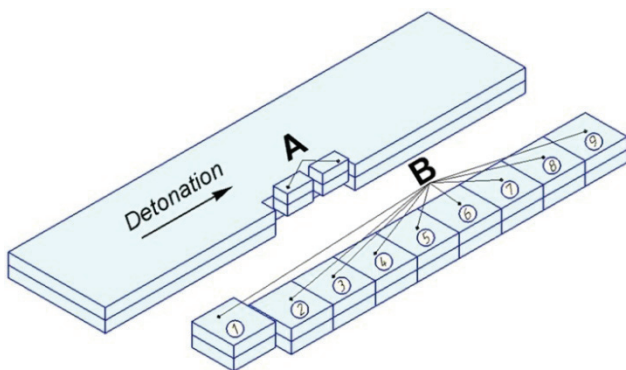


Fig. 3. Specimens for metallographic studies:  
A – specimens for metallographic study;  
B – specimens for tear strength study

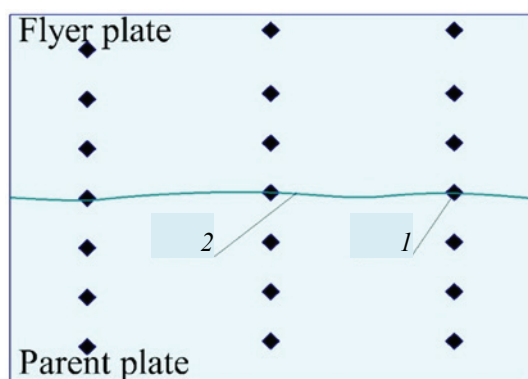


Fig. 4. Microhardness measurement diagram:  
1 – indention; 2 – weld interface

### 3. Results and Discussion

#### 3.1. Preliminary microstructural analysis

The calculated parameters for three different EW modes and the detonation velocities ( $D$ ) are listed in Table 2.

The mode 1 parameters did not produce a joint due to the insufficient plastic deformation of the surfaces and the insufficient pressure of the detonation products on the surface of the flyer plate.

Figure 6 shows the microstructure of the weld interface after etching for modes 2, 3. The weld interface produced by mode 2 (specimen 2) is in the shape of a nearly straight line (Fig. 6a), and the weld produced by mode 3 (specimen 3) is in the shape of a wave (Fig. 6b). Dark-etching structures were found along the weld interface (Figs. 6c and 6d). Supposedly, these structures are the accumulations of significantly deformed structures, which indicates the

Table 2. EW parameters

Mode	$r$	$D$ , m·s <sup>-1</sup>	$V_0$ , m·s <sup>-1</sup>	$\gamma$ , °
1	1.5	2000	600	17.2
2	2.6	2700	1100	23.6
3	3.7	3200	1535	27.8

presence of dislocations. The width of the dark-etching structures is 3–4  $\mu\text{m}$  (Fig. 6c and 6e) in specimen 2 and 7–9  $\mu\text{m}$  (Figs. 6d and 6f) in specimen 3.

Specimen 2 and especially specimen 3 show the presence of ASBs, which branch off from the weld interface into the material in both directions as shown by blue arrows in Figs. 6a and 6b. The ASBs are narrow regions of intense shear and plastic instability. They appear in materials after severe deformation.

In specimen 3, the number of ASBs increases due to higher impact velocity and higher deformation. In all the specimens, the angles between the ASBs and the weld interfaces are about 30°.

#### 3.2. EDS measurements

A detailed EDS analysis of the specimens before etching (points 6, 7 in specimens 2 in Fig. 7a and points 3–5 in specimens 3 in Fig. 7b) revealed structures with high Mg content (20.9–47.9 %), indicating the presence of  $\beta$ -phase in these structures. The Mg content in the  $\alpha$ -phase is about 7 % (points 1, 2 in specimen 2 in Fig. 7a and points 6 and 7 in Fig. 7b). Also, numerous (Fe, Mn)Al<sub>6</sub> inclusions (points 3 and 5 in Fig. 7a and points 1 and 2 in Fig. 7b) were observed.

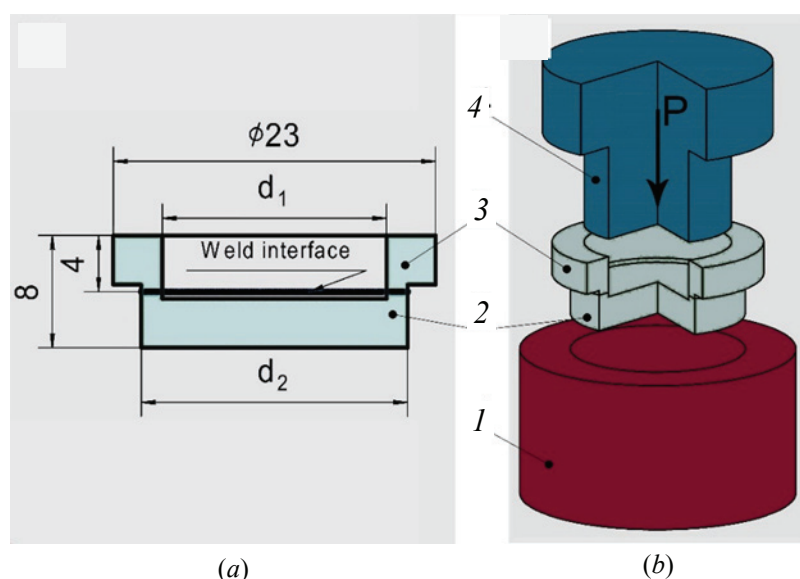
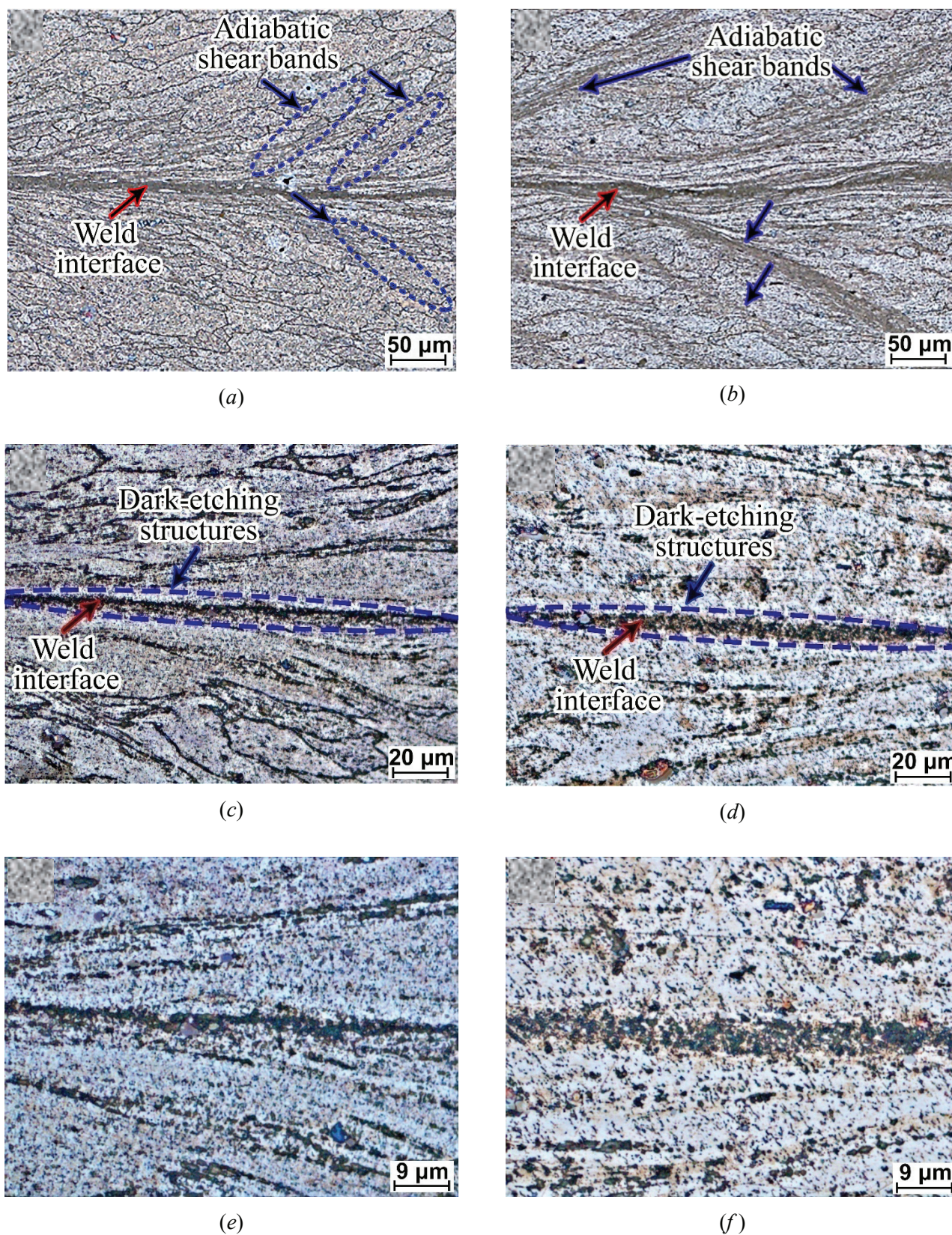


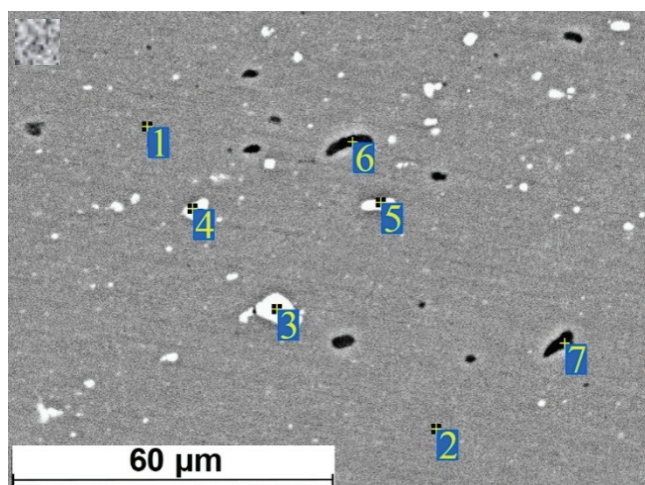
Fig. 5. Tear specimen (a) and tear testing diagram (b): 1 – mold; 2 – base layer; 3 – flyer layer; 4 – male die





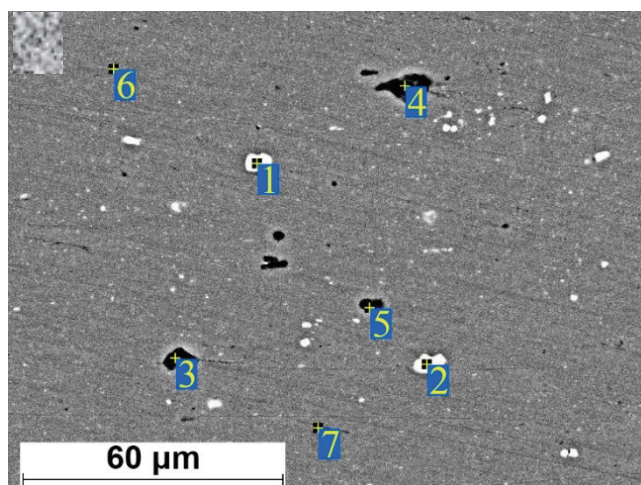
**Fig. 6.** Microstructure of the weld interface: specimen 2 (a, c, e) and specimen 3(b, d, f)





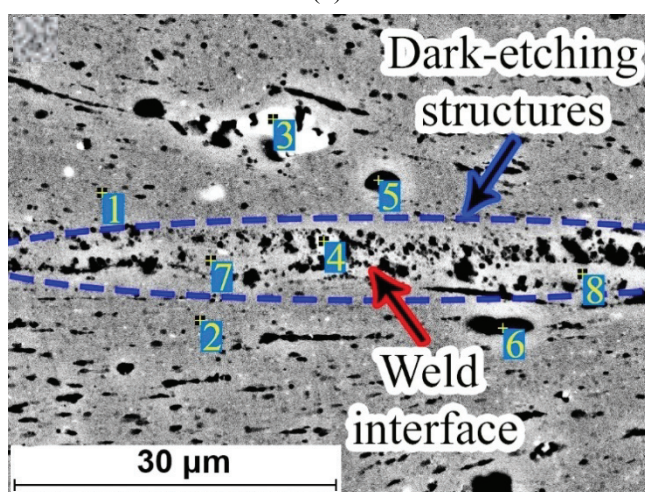
No.	O	Mg	Si	Mn	Fe	Al
Element content, at. %						
1	1.3	6.9	—	0.3	—	Balance
2	1.5	6.8	—	0.3	—	
3	1.5	0.6	1.7	6.8	7.8	
4	1.2	2.7	0.6	7.4	4.1	
5	2.1	2.2	2.7	5.6	7.5	
6	19.8	20.9	13.8	0.1	0.1	
7	28.6	32.4	18.3	—	0.1	

(a)



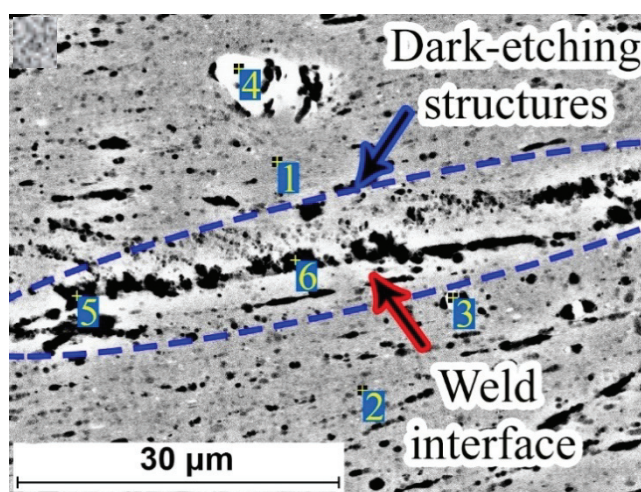
No.	O	Mg	Si	Mn	Fe	Al
Element content, at. %						
1	1.5	1.0	2.8	6.7	8.4	Balance
2	0.9	0.6	3.3	7.6	8.9	
3	24.0	15.9	15.1	0.1	0.1	
4	23.1	47.9	21.2	0.1	0.1	
5	24.7	35.1	17.1	—	—	
6	1.3	6.9	—	0.3	—	
7	0.8	6.9	—	0.3	—	

(b)



No.	O	Mg	Si	Mn	Fe	Al
Element content, at. %						
1	1.2	6.7	—	0.3	—	Balance
2	1.2	6.6	—	0.3	—	
3	1.3	2.0	0.8	4.4	6.9	
4	3.3	4.1	0.2	3.7	4.1	
5	0.4	7.1	0.1	0.5	0.1	
6	35.5	3.0	10.7	0.1	—	
7	1.0	6.7	0.1	0.4	—	
8	1.4	6.7	—	0.2	—	

(c)



No.	O	Mg	Si	Mn	Fe	Al
Element content, at. %						
1	1.2	6.5	—	0.3	—	Balance
2	1.3	6.6	—	0.2	—	
3	1.1	5.0	—	2.5	2.5	
4	1.4	1.3	2.6	6.3	7.7	
5	3.8	6.6	0.7	0.4	—	
6	4.2	6.6	0.1	0.3	—	

(d)

Fig. 7. SEM images of weld interface and the results of point EDS analysis: specimen 2 (a, c) and specimen 3 (b, d)

Figure 8 shows the points of microhardness distribution along the thickness of the specimens according to the diagram shown in Fig. 3. The dashed lines show the microhardness of the initial plate of AlMg6. The blue points indicate the microhardness of AlMg6–AlMg6 bimetal after EW. Both specimens exhibit a sharp decrease in microhardness at the weld interface. In some points, the microhardness is lower than in the initial plate. This decrease suggests that a dynamic recrystallization of the grains and an ageing of AlMg6 occurred due to extreme heating followed by rapid cooling of the weld interface. The sources of the heat are shock-compressed gas in the gap and severe plastic deformation of the surfaces during the collision. The recrystallization decreases the

dislocation density and therefore reduces the strength of the material [34].

After EW, the microhardness near the weld interface was approximately 200 HV, which was 20 % higher than that of the initial plate. This higher microhardness was due to work hardening in the initial plate. The width of the work-hardened zone was approximately 5 mm in specimen 1 and 2 mm in specimen 2.

The average tear strength in specimen 2 was  $(80 \pm 10)$  MPa, and in specimen 3 it was  $(230 \pm 10)$  MPa. The mechanical testing revealed three distinct zones of tear strength values. The first zone (Fig. 9) in specimens 2 and 3 had low tear strength ( $\leq 76$  MPa). This is due to the fact that it takes some

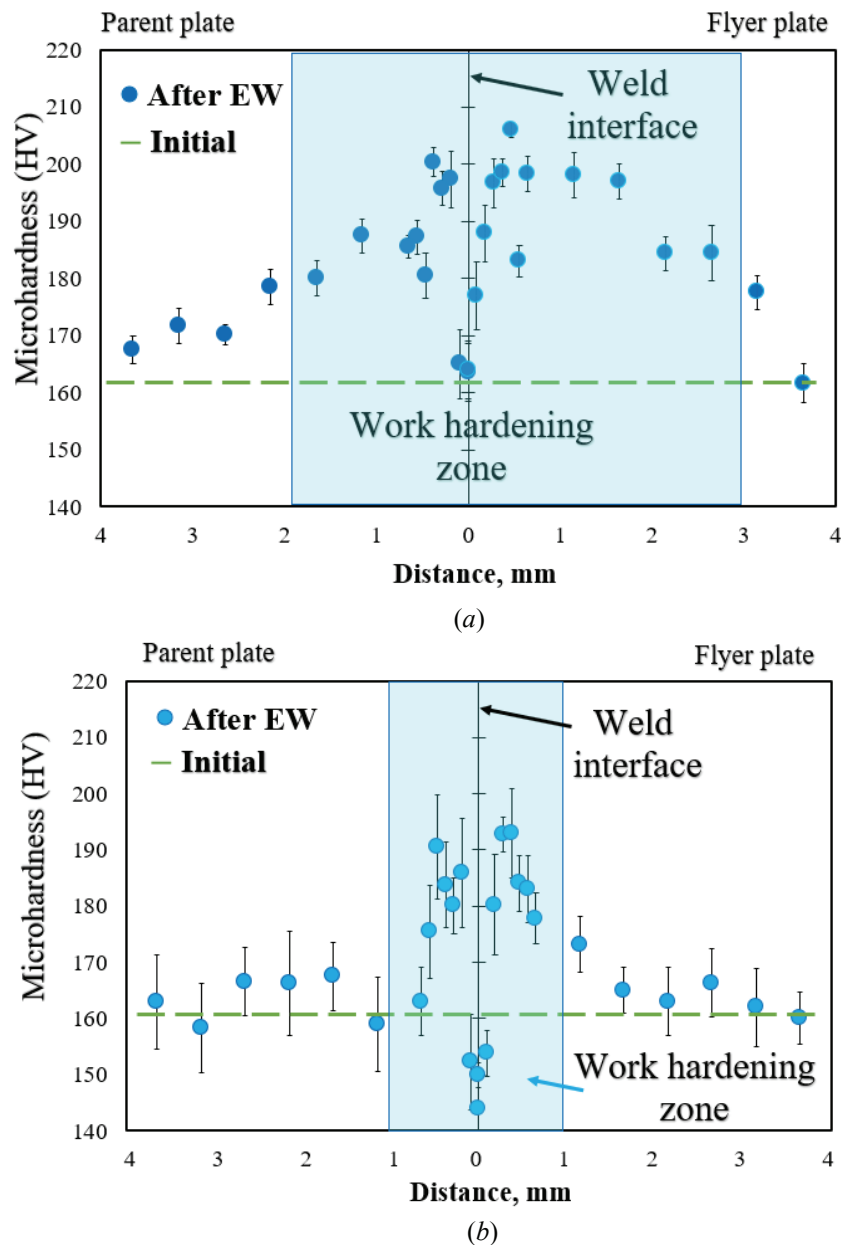


Fig. 8. Microhardness distribution in specimen 2 (a) and specimen 3 (b)



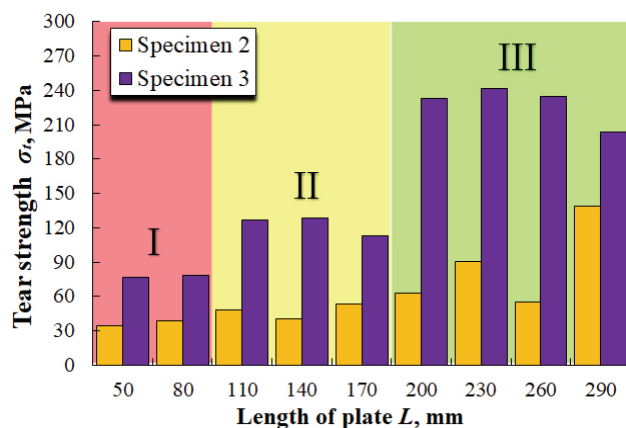


Fig. 9. The tear strength values distribution along the bimetal plates

time for the pressure to achieve the values that are necessary to form a strong joint. It is generally known that the high pressure and temperature in the welding gap provide removing both the oxide films and contaminants from the welded surfaces that make it possible for the atoms of two materials to meet at interatomic distance. Also, the pressure must be higher than the dynamic elastic limit of the materials for the deformation of the weld interface. At the beginning of the explosive welding process (it corresponds to the first zone) the pressure and temperature were not enough that to cleaning and deform the welded surfaces. The second zone shows a uniform tear strength distribution (113–128 MPa). The third zone had the highest tear strength values (204–242 MPa) and the average tear strength in this zone was 228 MPa, which was 35 % lower than the ultimate tensile strength of the initial AlMg6 plate.

As was noted earlier, welding a high-quality joint between Al–Mg alloys and stainless-steel using EW poses certain difficulties, which are caused by the formation of brittle intermetallic compounds at the weld interface and by  $\beta$ -phase ( $\text{Mg}_2\text{Al}_3$ ) along the boundaries of  $\alpha$ -phase [36]. In Al–Mg alloys, Mg provokes the formation of ASBs during deformation, which are zones of stress concentrations. ASBs then can transform into microcracks, which substantially reduces the strength of the material and its corrosion resistance. It should also be noted that with higher Mg content, ASBs form under lower deformations. In our previous studies [32], the EW joints between AlMg6 and 08Cr18Ni10Ti had the average tear strength of 120 MPa at most, which is not sufficient for the use as BTJs.

At present, much research has been focused on the use of friction stir welding (FSW) for obtaining BTJs, although this method has sample size restrictions [7]. EW does not have sample size restrictions; however, its pulse character of loading

substantially deforms the grains in the material and changes the structure of the weld interface.

In this study, EW experiments were carried out to study the evolution of the deformed microstructure of the weld interface as well as to detect the possible presence of diffusion of Mg from  $\alpha$ -phase and  $\delta$ -phase towards the weld interface. The possibility of diffusion of particles (atoms, impurity elements, etc.) under dynamic loading was explored in [45]. Moreover, EW of similar materials prevents forming IMCs and minimizes residual stresses at the weld interface.

The EW experiments with the parameter  $r = 1.5$  (specimen 1) did not result in an AlMg6–AlMg6 joint. This is probably due to the fact that a substantial amount of the explosive charge got scattered in the EW process thus reducing the pressure of the detonation products. This reduced pressure in its turn reduces the plastic deformation in the weld interface. The refractory oxide film on the AlMg6 surface also reduces the amount of plastic deformation. On the other hand, the parameters  $r = 2.6$  (specimen 2) and  $r = 3.7$  (specimen 3) produced an AlMg6–AlMg6 joint. The study of the microstructure of the weld interface shows that specimen 2 has a weld interface in the shape of an almost straight line (Fig. 6a), whereas specimen 3 has a weld interface in the shape of a wave. This wavy profile is due to higher EW parameters and as a result, stronger deformation of the weld interface in specimen 3. Chemical etching revealed dark-etching structures both in the weld interface and in the ASBs. The formation of ASBs is characteristic of Al–Mg alloys and with increasing Mg content their number usually increases.

Apparently, the dark-etching structures in the weld interface are accumulations of ultrafine IMCs. These IMCs before welding were along the grain boundaries, but the collision of the plates during the process of EW welding resulted in their accumulation in the weld interface. The etching revealed hollow surfaces of the dark-etching structures (Figs. 7c and 7d). These pits formed due to a higher solubility of nonmetallic inclusions in the etchant in areas with local accumulations of dislocations and the pitting of the surfaces of the specimens during grinding, which crushes the IMCs and dislodges them from the specimen surfaces.

Presumably, the plastic deformation caused by the EW process crushes the IMCs and move the fragments to the weld interface and to the zone adjacent to it. Notably, the highest concentration of the fragments is in the weld interface and it gradually decreasing further away from it.

The tear strength distribution along the bimetal plate (Fig. 9) shows that the average tear strength is not sufficiently high in specimen 2, thus mode 2 is not suitable for producing bimetals with an AlMg6 layer. On the other hand, the average tear strength is higher by 60 % in specimen 3, although its distribution along its length is not uniform.

#### 4. Conclusion

Optical and electron microscopy have revealed the presence of a large number of ASBs and dark-etching structures formed during EW. The number of the ASBs and dark-etching structures is roughly the same in both layers. The ASBs formed in the zones of maximum compressive stresses; the dark-etching structures are probably the accumulations of structural defects and IMC fragments. Tear testing of the weld joint has shown that higher EW parameters lead to much higher tear strength with a non-uniform distribution along the plate, which is attributed to the non-uniform impact of gaseous detonation products and the thermodynamic parameters of the shock-compressed gas. In order to achieve a joint between AlMg6 and various other alloys and metals with the highest strength possible, plastic deformation in the weld interface must be sufficiently high while the heating must be minimal. Based on the results of this study, optimal EW parameters could be developed in further studies to achieve a joint between AlMg6 and 08Cr18Ni10Ti steel with the strength close to that of AlMg6.

#### 5. Funding

This study received no external funding.

#### 6. Acknowledgements

This research was funded in accordance with the state task of Merzhanov Institute of Structural Macrokinetics and Materials Science of Russian Academy of Sciences (ISMAN). This research was performed using the set of modern scientific instruments available for multiple access at ISMAN Center of Shared Services. This research was performed using the set of modern scientific instruments available for multiple access at Polzunov Altai State Technical University Center of Shared Services.

#### 7. Conflict of interests

The authors declare no conflict of interest.

#### References

1. Wahid MA, Siddiquee AN, Khan ZA. Aluminum alloys in marine construction: characteristics, application, and problems from a fabrication viewpoint. *Marine Systems & Ocean Technology*. 2020;(15):70-80. DOI:10.1007/s40868-019-00069-w
2. Hosseinabadi OF, Khedmati MR. A review on ultimate strength of aluminium structural elements and systems for marine applications. *Ocean Engineering*. 2021;(232):109153. DOI:10.1016/j.oceaneng.2021.109153
3. Hirsch J. Aluminium in innovative light-weight car design. *Materials Transactions*. 2011;(52):818-824. DOI:10.2320/matertrans.L-MZ201132
4. Del Pero F, Delogu M, Berzi L, Dattilo CA, Zonfrillo G, Pierini M. Sustainability assessment for different design solutions within the automotive field. *Procedia Structural Integrity*. 2019;(24):906-925. DOI:10.1016/j.prostr.2020.02.080
5. Senkov ON, Bhat RB, Senkova SV. High strength aluminum alloys for cryogenic applications. *Metallic Materials with High Structural Efficiency*. 2004;146:151-162. DOI:10.1007/1-4020-2112-7\_15
6. Atabaki MM, Nikodinovski M, Chenier P, Ma J, Harooni M, Kovacevic R. Welding of aluminum alloys to steels: An overview. *Journal for Manufacturing Science and Production*. 2014;14(2):59-78. DOI:10.1515/jmsp-2014-0007
7. Ahmed MMZ, Jouini N, Alzahrani B, El-Sayed Seleman MMES, Jhaheen M. Dissimilar friction stir welding of AA2024 and AISI 1018: Microstructure and mechanical properties. *Metals*. 2021;(11):330. DOI:10.3390/met11020330
8. Vincze G, Simões F, Butuc M. Asymmetrical rolling of aluminum alloys and steels: A review. *Metals*. 2020;(10):1126. DOI:10.3390/met10091126
9. Shi H, Qiu R, Tu Y, Yu H, Yin D. Study on the joining characteristics of diffusion welding lap joint with various temperatures between aluminum alloy and stainless steel. *Advanced Materials Research*. 2011;291-294:1003-1006. DOI:10.4028/www.scientific.net/AMR.291-294.1003
10. Zhang C, Li H, Liu Q, Huang C, Zhou K. Ultrasonic welding of aluminum to steel: A review. *Metals*. 2023;13:29. DOI:10.3390/met13010029
11. Poddar VS, Rathod MJ. Evaluation of mechanical properties of cold roll bonded mild steel and aluminum. *Materials Today Proceedings*. 2021;43:3014-3022. DOI:10.1016/j.matpr.2021.01.363
12. Yu H, Tong Y. Magnetic pulse welding of aluminum to steel using uniform pressure electromagnetic actuator. *The International Journal of Advanced Manufacturing Technology*. 2017;91(5-8):2257-2265. DOI:10.1007/s00170-016-9928-y
13. Makhina DN, Nikulin SA, Denisov VN, Klyatskin AS. Effect of the production conditions on the structure and strength of the AlMg6 Alloy – 12Kh18N10T steel bimetallic joint. *Russian Metallurgy (Metally)*. 2020;(10):1095-1101. DOI:10.1134/S003602952010016X



14. Palaci Y, Olgun M. Influences of heat treatment on mechanical behavior and microstructure of the explosively welded grade steel / EN AW 5083 aluminium joint. *Archives of Metallurgy and Materials*. 2021;66(2):373-380. DOI:10.24425/amm.2021.135868
15. Carvalho GHSFL, Galvão I, Mendes R, Leal RM, Loureiro A. Explosive welding of aluminium to stainless steel using carbon steel and niobium interlayers. *Journal of Materials Processing Technology*. 2020;283:116707. DOI:10.1016/j.jmatprotec.2020.116707
16. Wang J, Zhang Y. A study on weldability of aluminum alloy-aluminum-steel transition joints. *Advanced Materials Research*. 2013;631-632:713-716. DOI:10.4028/www.scientific.net/AMR.631-632.713
17. Boroński D, Skibicki A, Maćkowiak P, Płaczek D. Modeling and analysis of thin-walled Al/steel explosion welded transition joints for shipbuilding applications. *Marine Structures*. 2020;74:102843. DOI:10.1016/j.marstruc.2020.102843
18. Matteis P, Gullino A, D'Aiuto F, Puro CM, Scavino G. Welding between aluminum alloy and steel sheets by using transition joints. *Journal of Materials Engineering and Performance*. 2020;29:4840-4853. DOI:10.1007/s11665-020-04595-2
19. Costanza G, Crupi V, Guglielmino E, Sill A, Tata ME. Metallurgical characterization of an explosion welded aluminum/steel joint. *Metallurgia Italiana*. 2016;108(11):17-22.
20. Li X, Ma H, Shen Z. Research on explosive welding of aluminum alloy to steel with dovetail grooves. *Materials & Design*. 2015;87:815-824. DOI:10.1016/j.matdes.2015.08.085
21. Wang J, Li X-Jie, Yan H-Hao, Wang X-Hong, Wang Y-Xin. Research on titanium-copper explosive welding interface with different welding parameters. *International Journal of Advanced Manufacturing Technology*. 2022;122(9-10):3595-3606. DOI:10.1007/s00170-022-10102-9
22. Raj P, Ramya DG, Manoj Kumar VK, Suresh OP. Tensile and shear strength evaluation in joining dissimilar plates of mild steel with aluminum alloy through explosive cladding approach. *Materials Today*. 2023;80:2753-2759. DOI:10.1016/j.matpr.2021.07.032
23. Chen X, Inao D, Tanaka S, Mori A, Li X, Hokamoto K. Explosive welding of Al alloys and high strength duplex stainless steel by controlling energetic conditions. *Journal of Manufacturing Processes*. 2020;58:1318-1333. DOI:10.1016/j.jmapro.2020.09.037
24. Kwiecien M, Kopyscianski M, Bloniarz R, Muszka K, Majta J. Influence of deformation conditions on the in homogeneity of plastic flow of structurally graded bimetal systems. *Procedia Manufacturing*. 2018;15:1649-1655. DOI:10.1016/j.promfg.2018.07.272
25. Grinberg BA, Ivanov MA, Rybin VV, Elkina OA, Patselov AM, Antonova OV, Inozemtsev AV, Tolmachev TP. Fragmentation processes during explosion welding (review). *Russian Metallurgy (Metally)*. 2013;727-737. DOI:10.1134/S0036029513100030
26. Greenberg BA, Ivanov MA, Kuzmin SV, Lysak VI. *Explosive welding: Processes and structures*. 1st ed. Boca Raton: CRC Press; 2019. 242 p. DOI:10.1201/9780429340550
27. Rouzbeh A, Sedighi M, Hashemi R. Comparison between explosive welding and roll-bonding processes of AA1050/Mg AZ31B bilayer composite sheets considering microstructure and mechanical properties. *Journal of Materials Engineering and Performance*. 2020;29:6322-6332. DOI:10.1007/s11665-020-05126-9
28. Fang Z, Shi C, Shi H, Sun Z. Influence of explosive ratio on morphological and structural properties of Ti/Al clads. *Metals*. 2019;9:119. DOI:10.3390/met9020119
29. Zerui S, Changgen S, Zhonghang F, Hang S. A dynamic study of effect of multiple parameters on interface characteristic in double-vertical explosive welding. *Materials Research Express*. 2020;7:016541. DOI:10.1088/2053-1591/ab6538
30. Bugajska M, Maj L, Jarzebska A, Terlicka S, Faryna M, Szulc Z, Wojewoda-Budka J. Variety of aluminum/steel interface microstructures formed in explosively welded clads followed by the weld's thermal expansion response. *Journal of Materials Engineering and Performance*. 2022;31:7088-7097. DOI:10.1007/s11665-022-07027-5
31. Sherpa BB, Kumar PD, Upadhyay A, Kumar A, Agarwal A, Tyagi S. Effect of explosive welding parameters on Al/LCS interface clad by low velocity of detonation explosive welding (LVEW) process. *International Journal of Advanced Manufacturing Technology*. 2021;113(11-12):3303-3317. DOI:10.1007/s00170-021-06800-5
32. Malakhov AY, Saikov IV, Denisov IV, Niyozbekov NN. AlMg6 to titanium and AlMg6 to stainless steel weld interface properties after explosive welding. *Metals*. 2020;(10):1500. DOI:10.3390/met10111500
33. Trikov YP, Gurevich VG, Shmorgunov VG. *Layered composites based on aluminum and its alloys*. Moscow: Metallurgizdat; 2004. 230 p. (In Russ.)
34. Ambroziak A, Korzeniowski M, Kustron P, Winnicki M, Sokołowski P, Harapinska E. Friction welding of aluminium and aluminium alloys with steel. *Advances in Materials Science and Engineering*. 2014;1-15. DOI:10.1155/2014/981653
35. Grignon F, Benson D, Vecchio KS, Meyers MA. Explosive welding of aluminum to aluminum: analysis, computations and experiments. *International Journal of Impact Engineering*. 2004;30:1333-1351. DOI:10.1016/j.ijimpeng.2003.09.049
36. Ren L, Gu H, Wang W, Wang S, Li C et al. Effect of mg content on microstructure and properties of Al-Mg alloy produced by the wire arc additive manufacturing method. *Materials*. 2019;(12):4160. DOI:10.3390/ma12244160
37. Saikov IV, Malakhov AY, Saikova GR, Denisov IV, Gulyaev PYu. Influence of explosive welding parameters on the structure of interface in brass-invar thermobimetal. *Inorganic Materials: Applied Research*. 2020;(11):448-452. DOI:10.1134/S2075113320020331
38. George F, Vander V. *ASM Handbook: Metallography and Microstructures*. 9th ed. United States: ASM International; 2004. 1184 p.

39. Thomas J, Bruno Dehua Y, Mueller E, George F, Vander V, Jeffrey AJ, Magdefrau N, Deacon R. *Materials characterization*. 10nd ed. United States: ASM International; 2019. 800 p.

40. Berdychenko AA, Guryev AM, Ivanov SG, Guryev MA, Sitnikov AA. Morphology of layered metal composites, obtained in various ways. *Fundamental'nyye problemy sovremennogo materialovedeniya*. 2021;2:216-223. (In Russ.)

41. Kazakov AA, Ryaboshuk SV, Lyubochko DA, Chigintsev LS. Research on the origin of nonmetallic inclusions in high-strength low-alloy steel using automated feature analysis. *Microscopy and Microanalysis*. 2015;(21):1755-1756. DOI: 10.1017/S1431927615009551

42. Vander Voort GF, Pakhomova O, Kazakov A. Evaluation of normal versus non-normal grain size

distributions. *Materials Performance and Characterization*. 2016;5(5). DOI:10.1520/MPC20160001

43. Kazakov AA, Kiselev D. Industrial application of thixomet image analyzer for quantitative description of steel and alloy's microstructure. *Metallography, Microstructure, and Analysis*. 2016;5(4):294-301. DOI:10.1007/s13632-016-0289-6

44. Kazakov AA, Kovalev P, Ryaboshuk S. Metallurgical expertise as the base for determination of nature of defects in metal products. *CIS Iron and Steel Review*. 2007;(1-2):7-13.

45. Buravova SN, Petrov EV. Acceleration of mass transfer under dynamic loading. *Russian Journal of Physical Chemistry B*. 2018;12:120-128. DOI:10.1134/S1990793118010153

### Information about the authors / Информация об авторах

**Andrey Yu. Malakhov**, Cand. Sc. (Eng.), Senior Researcher, Merzhanov Institute of Structural Macrokinetics and Materials Science Russian Academy of Sciences (ISMAN), Chernogolovka, Russian Federation; ORCID0000-0002-0567-7307; e-mail: sir.malahov2009@yandex.ru

**Ivan V. Saikov**, Cand. Sc. (Eng.), Leading Researcher, Deputy director of the ISMAN, Chernogolovka, Russian Federation; ORCID 0000-0003-1473-2854; e-mail: revan.84@mail.ru

**Igor V. Denisov**, Cand. Sc. (Eng.), Researcher, ISMAN, Chernogolovka, Russian Federation; ORCID 0000-0002-1065-3318; e-mail: ingener.denisov@yandex.ru

**Alexander A. Berdychenko**, Cand. Sc. (Eng.), Associate Professor, Head of the Department of the Polzunov Altai State Technical University (ASTU), Barnaul, Russian Federation; e-mail: berd50@mail.ru

**Sergey G. Ivanov**, D. Sc. (Eng.), Leading Researcher of the ASTU, Barnaul, Russian Federation; ORCID 0000-0002-5965-0249; e-mail: serg225582@mail.ru

**Nemat N. Niyozbekov**, Junior Researcher, ISMAN, Chernogolovka, Russian Federation; ORCID0000-0003-1812-2930; e-mail: nemat199595@mail.ru

**Малахов Андрей Юрьевич**, кандидат технических наук, старший научный сотрудник, ФГБУН «Институт структурной макрокинетики и проблем материаловедения им. А. Г. Мерджанова Российской академии наук (ИСМАН), Черноголовка, Российская Федерация; ORCID 0000-0002-0567-7307; e-mail: sir.malahov2009@yandex.ru

**Сайков Иван Владимирович**, кандидат технических наук, ведущий научный сотрудник, заместитель директора по научной работе ИСМАН, Черноголовка, Российская Федерация; ORCID 0000-0003-1473-2854; e-mail: revan.84@mail.ru

**Денисов Игорь Владимирович**, кандидат технических наук, научный сотрудник, ИСМАН, Черноголовка, Российская Федерация; ORCID 0000-0002-1065-3318; e-mail: ingener.denisov@yandex.ru

**Бердыченко Александр Анатольевич**, кандидат технических наук, доцент, заведующий кафедрой современных специальных материалов, Алтайский государственный технический университет им. И. И. Ползунова (АлтГТУ), Барнаул, Российская Федерация; e-mail: berd50@mail.ru

**Иванов Сергей Геннадьевич**, доктор технических наук, ведущий научный сотрудник, АлтГТУ, Барнаул, Российская Федерация; ORCID 0000-0002-5965-0249; e-mail: serg225582@mail.ru

**Нийёзбеков Нёмат Нийёзбекович**, младший научный сотрудник, ИСМАН, Черноголовка, Российская Федерация; ORCID 0000-0003-1812-2930; e-mail: nemat199595@mail.ru

Received 18 September 2023; Accepted 03 November 2023; Published 15 December 2023



**Copyright:** © Malakhov AY, Saikov IV, Denisov IV, Berdychenko AA, Ivanov SG, Niyozbekov NN, 2023. This article is an open access article distributed under the terms and conditions of the Creative Commons Attribution (CC BY) license (<https://creativecommons.org/licenses/by/4.0/>).